Journal of Optoelectronics and Advanced Materials Vol. 3, no. 4, December 2001, p. 817 - 830

REVIEW PAPER

REMOTE SENSING OF THE SOUTHERN OCEAN: TECHNIQUES AND RESULTS

R. Barbini, F. Colao, R. Fantoni, L Fiorani, A. Palucci

ENEA, Via Fermi 45, 00044 Frascati, Italy

A lidar fluorosensor was developed in the framework of the Italian Antarctic Research Program. This system and some ancillary instruments were installed in the research vessel *Italica* during three oceanographic campaigns in the Southern Ocean and collected data on biochemical parameters of the seawaters crossed. In particular, thematic maps of chlorophyll-a and chromophoric dissolved organic matter have been released, thus providing information on phytoplankton dynamics. Moreover, the chlorophyll-a measurements have been used for calibrating the satellite imagery.

(Received July 9, 2001; accepted November 29, 2001)

Keywords: Remote sensing, Lidar fluorosensor, Satellite radiometer, Oceanography, Antarctica

1. Introduction

The climate equilibrium is influenced by the global carbon cycle in the biosphere. Oceans play a major role in this process: phytoplankton is responsible for about 40% of the global carbon fixation, commonly indicated as primary productivity [Falkowski and Raven, 1997]. Climatic conditions, nutrient availability and physical forcings are functions of space and time. Their cycles explain the large variability of aquatic photosynthetic organisms. In particular, the Southern Ocean is an important sink for atmospheric CO_2, due to the cooling of warm subtropical waters and to the utilization of nutrient-rich up-welling deep waters. In Antarctic seas, rapid seasonal phytoplankton blooms may occur during the ice pack melting, especially in polynya areas near the coast [Lazzara et al., 1999]. In general, the phytoplankton biomass can be estimated from chlorophyll-a measurements.

Chromophoric dissolved organic matter (CDOM) arises from phytoplankton degradation and exudation following intense blooms. It is constituted by different complex compounds, mainly humic and fulvic acids, and acts as a regulator of the algal growth, limiting the light penetration and thus reducing the photosynthesis [Olaizola et al., 1996]. The optical characterization of these substances is complicated because of their predisposition to develop superficial microlayers [Carlson and Mayer, 1980] that evolve upon sun illumination.

Remote sensing of seawaters can be either passive [Elachi, 1987], based on the sun as a light source, or active [Measures, 1992], assisted by lamps or lasers. The passive technique relies on observing the ocean color, i.e. on measuring the sunlight backscattered by the water surface at different wavelengths. It suits especially satellite borne sensors. As a consequence, it provides global coverage but requires atmospheric corrections, since the contribution of air molecules and aerosols (about 80%) should be subtracted from the sensed radiance. The active method is usually based on the laser induced fluorescence (LIF), e.g. chlorophyll-a is detected measuring its fluorescence emission at around 680 nm excited by an ultraviolet (UV) laser beam, e.g. at 355 nm. The latter technique has been applied to air or ship borne sensors, thus supplying "in situ" measurements (sea truth). It is actually limited by its local coverage: it could takes years for a plane or a ship to sample a region sensed in minutes by a satellite.

Lidar fluorosensors are probably the more common LIF instruments and have been extensively operated to monitor sea [Reuter et al., 1993] and land [Edner et al., 1995]. LIF spectra contain signatures of phytoplankton, CDOM and dispersed impurities, such as crude oils [Bristow et al., 1981; Hoge and Swift, 1981; Koechler et al., 1992]. Lidar fluorosensors can be used to determine the concentration of the different phytoplankton pigments, thus allowing for the assignment of relevant algae to coarse classes [Barbini et al., 1998]. When operated in the pump-and-probe emission mode [Chekalyuk et al., 1993], a lidar fluorosensor can determine the chlorophyll-a fluorescence yield, a parameter related to the photosynthetic electron transport under actual environmental conditions (nutrient availability, sun illumination, salinity, pH, presence of toxic substances, etc.). Thanks to narrowband filtering and electronic gating, LIF signals do not need corrections for radiometric and spectral characteristics of solar irradiance and surface reflectance. Furthermore, due to the short distance from the target (few meters), atmospheric effects are negligible.

In this paper, we review the main characteristics of a passive and an active sensor, the Sea-viewing Wide Field-of-view Sensor (SeaWiFS) [Hooker et al., 1992] and the ENEA Lidar Fluorosensor (ELF) [Barbini et al., 1999; Barbini et al., 2001], respectively. In particular, the chlorophyll-a and CDOM data gathered by ELF during three oceanographic campaigns (XIII: December 1997 – January 1998, XV: January 2000 – February 2000 and XVI: January 2001 – February 2001) in the Ross Sea are discussed. Finally, the ELF measurements are used for a new calibration of the SeaWiFS chlorophyll-a bio-optical algorithm in the Southern Ocean.

2. Techniques

2.1 A passive remote sensor: SeaWiFS

The first observations of ocean color from space were carried out by the Coastal Zone Color Scanner (CZCS) [Cracknell et al., 2001], operated on the Nimbus-7 satellite from 1978 to 1986. CZCS permitted a dramatic advance in our understanding of the oceanic processes. The water-leaving radiance was measured in 6 bands (4 visible and 2 infrared).

Sea WiFS is the follow-on sensor to CZCS. It was launched on August 1, 1997 aboard the OrbView-2 satellite and data acquisition started on September 4, 1997. While CZCS recorded scenes less than 27 min. per day (approximately 1/4 of pole-to-pole orbital swath), SeaWiFS operates full time (around 15 pole-to-pole orbital swaths per day) scanning approximately 90% of the oceans every two days. Other improvements include more detection bands, higher signal-to-noise ratios, better atmospheric corrections and more reliable bio-optical algorithms. The goal of SeaWiFS is to examine oceanic factors that affect global change. In particular, an accuracy to within 35% for chlorophyll-a concentration over the range of 0.05-50 mg m^{-3} should be achieved. The main characteristics of OrbView-2 and SeaWiFS are listed in Tables 1 and 2.

Table 1. Nominal operating parameters for OrbView-2 and SeaWiFS.

Orbit	Sun-synchronous
Altitude	705 km
Equator Crossing	Noon ± 20 min., descending node
Inclination	98° 12’
Orbital Period	98.9 min.
Scan Width	58°.3 (LAC[1]); 45°.0 (GAC[2])
Scan Coverage	2,800 km (LAC); 1,500 km (GAC)
Pixels along Scan	1,285 (LAC); 248 (GAC)
Nadir Resolution	1.13 km (LAC); 4.5 km (GAC)
Scan Period	0.167 s
Tilt	20°, 0°, +20°
Digitization	10 bits

[1]LAC: Local Area Coverage
[2]GAC: Global Area Coverage

The sunlight backscattered by both the Earth’s surface and the atmosphere is collected by an off-axis folded telescope and reflected to a rotating half-angle mirror. The radiation is then directed through dichroic beam splitters (separation into 4 wavelength regions) and spectral bandpass filters (narrowing of the 4 regions to the 8 bands), then impinges on silicon detector elements. The electronics module performs amplification, analog-to-digital conversion and time delay and integration for data transmission. The calibration is ensured by a solar radiation diffuser and the lunar observation. The sensor may be tilted forward or backward 20° along the orbit to minimize direct sunglint (mirror-like reflection of the air-water interface).

Table 2. Nominal radiometric parameters for SeaWiFS.

Band	Center Wavelength [nm]	Primary Use
1	412 (violet)[1]	Dissolved Organic Matter (DOM) included gelbstoffe
2	443 (blue)[1]	Chlorophyll-a absorption
3	490 (blue-green)[1]	Pigment absorption (Case II water[2]), K(490)[3]
4	510 (blue-green)[1]	Chlorophyll-a absorption
5	555 (green)[1]	Optical properties, pigments, sediments
6	670 (red)[1]	Atmospheric correction (CZCS heritage)
7	765 (near IR)[1]	Atmospheric correction, aerosol radiance
8	865 (near IR)[1]	Atmospheric correction, aerosol radiance

[1]Bands 1-6: bandwidth of 20 nm. Bands 7-8: bandwidth of 40 nm.
[2]Case I water is clear (open ocean): its optical properties are dominated by chlorophyll-a. Case II water is turbid (coastal): its optical properties are dominated by pigments other than chlorophyll-a.
[3]Diffuse attenuation coefficient at 490 nm (measure of optical clarity).

Data processing for chlorophyll-a retrieval consists mainly of two steps: atmospheric corrections [Gordon and Wang, 1994; Fiorani et al., 1998] and bio-optical algorithms [O'Reilly et al., 1998; Sathyendranath et al., 2001]. Atmospheric corrections are necessary to obtain the water-leaving radiance, removing from the sensor measurements the contributions of air molecules and aerosols, which typically represent about 80% of the total in the visible bands. Usually, they are based on the experimental observation that the water-leaving radiance is negligible for the longer wavelengths (red and near infrared). In these spectral regions the contributions of air molecules and aerosols can be directly obtained from the sensor measurements. Atmospheric corrections for the longer wavelengths are then combined with the predictions of models and applied to visible bands. Bio-optical algorithms consist of some semi-empirical equations used to calculate chlorophyll-a concentrations from the water-leaving radiances in the visible bands. Sunlight is not merely reflected by the water surface, but – after entering the ocean – it is selectively absorbed and scattered by phytoplankton and then backscattered through the water surface. This approach permits quantitative estimates of chlorophyll-a concentrations within the upper tens of meters of the open ocean and for minor depths in coastal zones. Due to large differences in absorption, data processing must be calibrated through "in situ" measurements. For SeaWiFS this is accomplished by a Marine Optical Buoy (MOBY) moored off the cost of Hawaii and by dedicated cruises.

2.2 An active remote sensor: ELF

ELF (Fig. 1) usually takes part to oceanographic campaigns, during Antarctic missions. It is a part of a complete laboratory, including local and remote instruments for continuous monitoring and local sampling, lodged into a ISO 20' container installed on the research vessel (R/V) *Italica*. The lidar fluorosensor, capable of normal or pump-and-probe operation [Chekalyuk et al., 1993], is assisted by ancillary instruments: a lamp spectrofluorometer, a pulsed amplitude fluorometer (PAM), a solar radiance detector and a global positioning system (GPS).

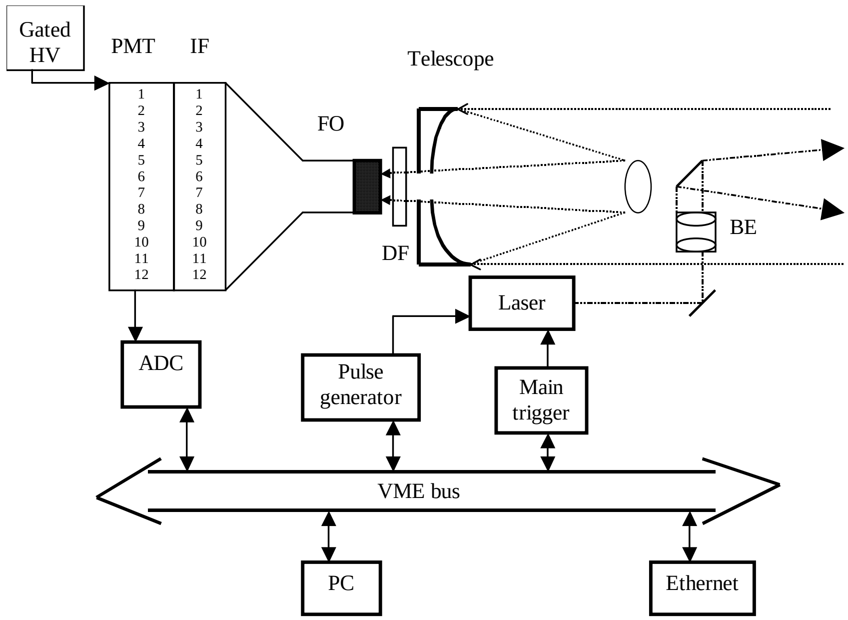

Fig. 1. Layout of ELF.

The light source is a frequency-tripled Nd:YAG laser (355 nm) followed by a beam expander (BE). ELF transmits the exciting pulse and receives the generated radiation through an optical window and an external mirror in order to reach the sea surface at normal incidence. The optical signal, after collection by a telescope, traverses a dichroic filter (DF), rejecting most of the laser beam, and is forwarded by a multi-arm fiber optic (FO) to interference filters (IFs). After spectral selection, photomultiplier tubes (PMTs) perform the detection. Their electronic output is digitized by analog-to-digital converters (ADCs). A personal computer (PC), embedded in a Versa Module Eurocard (VME) bus, controls all the experimental settings, including the normal or pump-and-probe excitation, the laser transmitter energy, the PMTs high voltage (HV) and gating time and the data acquisition parameters.

The beam footprint on the sea surface is a circle of about 0.2 m diameter and the data are time integrated for 5 s. Taking into account the average speed of the R/V, each data point taken by ELF correspond to an approximately 0.2 m wide and 12 m long track. The main spectral channels have a full width at half maximum (FWHM) of 5 nm and are centered at 402, 450 and 680 nm, corresponding to water Raman backscattering, CDOM and chlorophyll-a fluorescence, respectively.

In the case of homogeneous seawater, assuming a linear regime for the laser excitation and a low chromophore density for all the species present (natural offshore seawater), saturation can be neglected. The space integration on the investigated water column generates a total time integrated LIF signal $F(\lambda_{em})$, which can be expressed as [Measures, 1992]

$$F(\lambda_{\mathrm{em}}) = \frac{A(R_0)}{m^2} E_{ex} \frac{\sigma(\lambda_{em}, \lambda_{ex})}{k_T}, \tag{1}$$

where λ_{em} (λ_{ex}) stands for the emission (excitation) wavelength, m is the refraction index of water, $A(R_0)$ is a constant embedding the system parameters and changing with the distance R_0 from the water surface, E_{ex} is the excitation energy, σ is the fluorescence efficiency, $k_T = k_{ex} + k_{em}$ is the total extinction coefficient, resulting from extinction terms at the excitation and emission wavelength.

In order to evaluate concentrations of different chromophores dispersed in water, LIF signals can be calibrated against the concurrent water Raman signal, regarded as an internal standard reference [Bristow et al., 1981]. By rationing the chromophore fluorescence signal F to the water Raman intensity R, we have [Hoge and Swift, 1981]

$$\frac{F}{R} = \frac{\sigma_F}{\sigma_R} \frac{k_{ex} + k_R}{k_{ex} + k_F}, \tag{2}$$

where the indexes are self-explaining and the dependence on system parameters and on the refraction index of water has disappeared. The ratio of extinction coefficients in equation (2) can approximately be regarded as a constant and thus neglected, provided that a careful choice of excitation and emission wavelengths is performed, in order to avoid errors due to differential absorption. In conclusion, the different chromophore concentrations, expressed in Raman units, are taken as independent of system parameters. The transformation from Raman units to μg/l is performed by calibration with conventional techniques in some selected points.

The main characteristics of ELF are listed in Table 3. More details on ELF, the ancillary instruments, the measurement principle, the calibration procedure and the results obtained with the pump-and-probe excitation were previously given [Barbini et al., 1999; Barbini et al., 2001]. In this paper, the discussion is focused on the data gathered by ELF during three oceanographic campaigns in the Ross Sea (XIII: December 1997 – January 1998, XV: January 2000 – February 2000 and XVI: January 2001 – February 2001) and on the use of ELF measurements for a new calibration of the SeaWiFS chlorophyll-a bio-optical algorithm in the Southern Ocean.

Table 3. Typical specifications of ELF.

Transmitter	Laser	Nd:YAG
	Wavelength	355 nm
	Pump pulse energy	30 mJ
	Probe pulse energy	3 mJ
	Pulse duration	10 ns
	Pulse repetition rate	10 Hz
	Beam expansion	1 x – 20 x
Receiver	Telescope	Cassegrain
	Clear aperture	0.4 m
	Focal length	1.65 m
	Fiber optic length	1 m
	Fiber optic diameters	Input 25.4 mm, output 7 mm
	Interferential filters center wavelength	402, 450, 650, 680 nm
	Interferential filters bandwidth	5 nm FWHM
	Photomultiplier tubes	Hamamatsu R3896, R1477, R928
	Gated High Voltage	100 – 200 ns
Electronics	Bus	ISA-VME mixed bus
	ADC	CAEN V265 (15 bit)
	Computer	VME-CPU embedded 486-100 MHz

3. Results

3.1 ELF data

The western Ross Sea (Fig. 2), in proximity to the Italian base at Terra Nova Bay (TNB), represented the main investigated area during the oceanographic surveys on board of the R/V *Italica*, together with the transects up to New Zealand.

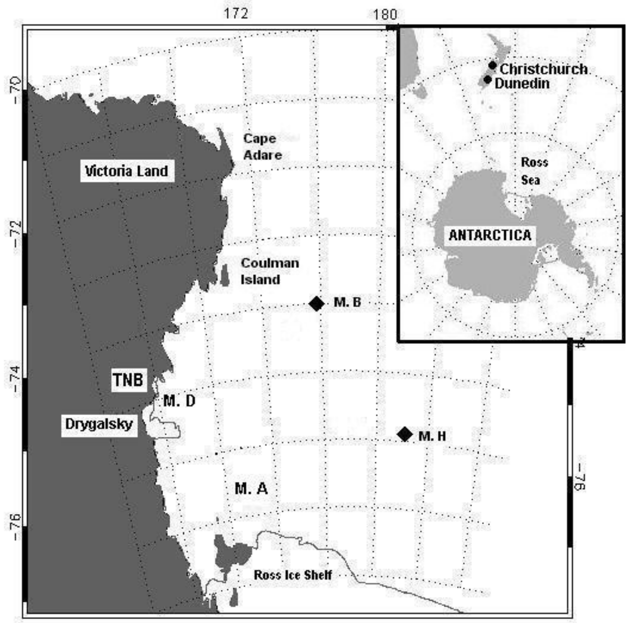

Fig. 2. Map of the investigated area (western Ross Sea). The location of the main sampling sites is indicated, as reported in Table 4. The Southern Ocean separates New Zealand and Ant arctica (inset).

Seasonal phytoplanktonic outgrowths dominate the wide area crossed in the Ross Sea, which is covered by ice pack for long periods, with temporal and spatial behavior largely driven by environmental parameters such as pressure, temperature, available solar radiation and katabatic winds. As a consequence of such physical forcing, two different scenarios were monitored during the XIII and XVI Antarctic expeditions. Both campaigns were dominated by the ice pack melting and the following prompt algal blooms, but with a different time phase. ELF data of chlorophyll-a are given for both campaigns as thematic maps (Fig. 3). During the XIII campaign (A), springtime started at the end of November 1997 and the corresponding lidar determinations of high chlorophyll concentrations appear to be in agreement with the expected seasonal behavior. In contrast, an exceptionally delayed springtime was observed at the end of January 2001, during the XVI campaign. ELF revealed abundance of phytoplankton in the southern side of the Ross Sea (B), when the area was completely free from ice coverage, while the central part (72° – 74° S) was still occupied by ice pack and icebergs.

In general, in the Ross Sea the CDOM content is much lower than that to continental waters and dissolved and particulate phases reaches approximately 10% and 90% of the total organic matter respectively [Carlson et al., 2000]. In the Antarctic inner basins, the continental ice melting and the large bloom evolution both contribute remarkably the CDOM stocks. ELF data of CDOM are given for both campaigns as thematic maps (Fig. 4). The CDOM distributions reveal the presence of higher values in polynya and in the southern areas close to the Drygalsky and Ross ice-shelf, with a minor content in the offshore seawaters. Throughout the XIII campaign, the overall CDOM content was five times higher than that to the XVI campaign. The presence of ice limited the superficial organic matter development in the latter case. Data of the XV campaign have not been shown for the sake of simplicity. During that campaign, the Ross Sea was in a diffused post bloom situation due to the ice melting.

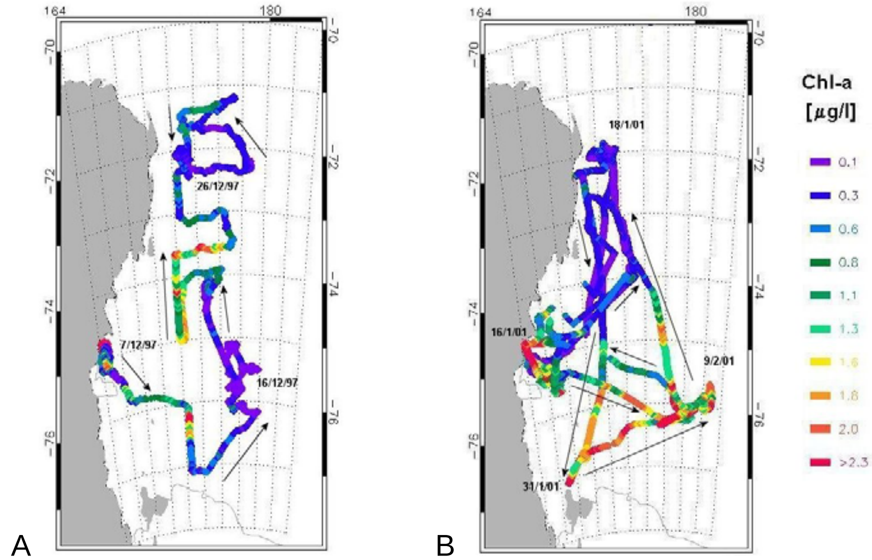

Fig. 3. Map of the superficial chlorophyll-a in the Ross Sea. A) 07/12/97 – 26/12/97. B) 12/01/01 – 15/02/01. The color code is in µg/l.

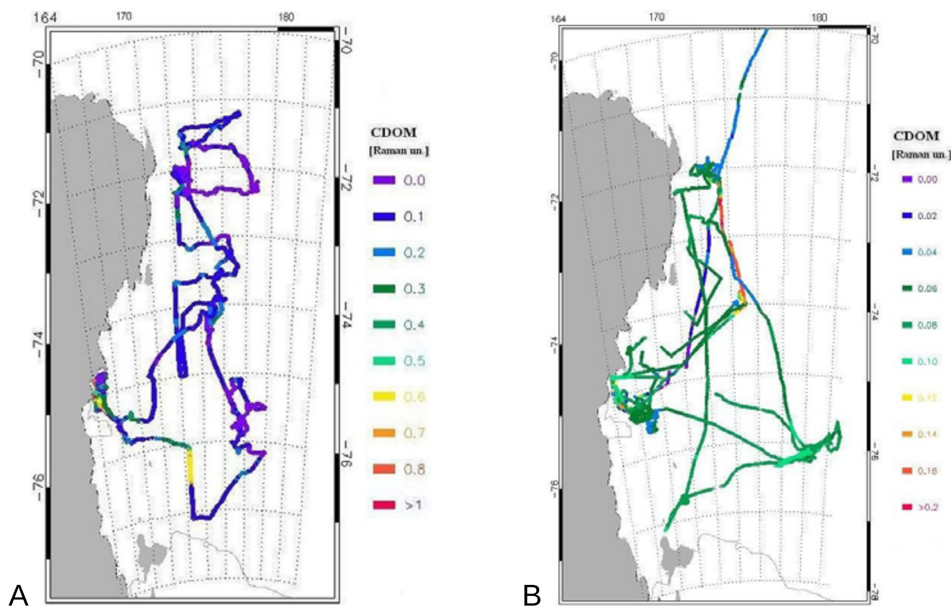

Fig. 4. Map of the superficial CDOM in the Ross Sea. A) 07/12/97 – 26/12/97. B) 12/01/01 – 15/02/01. The color code is in Raman units. Note that in B) the scale is reduced five times.

ELF data collected in correspondence of hydrographic moorings or other representative sites are summarized in Table 4. In general, the seasonal changes are influenced by strong katabatic winds, blowing off the Antarctic continent and inducing breaks and movements of the ice-pack, and by the concurrent increase in solar irradiance during springtime [Smith et al., 1996]. Data obtained in the XIII and XVI campaigns, confirm the suggested mechanism for seasonal phytoplankton cycles. Namely, intense springtime phytoplanktonic blooms of *Phaecocystis antarctica* [Innamorati et al., 1999] were detected in polynya areas (TNB) in both campaigns, with a spread of the outgrowth in the area near the Drygalsky ice tongue, including the neighborhood of mooring D. This evidence is also confirmed by the concurrent increase in CDOM, due to the ongoing rise of degradation substances and accessory pigments dominating the blue emission. The northern Ross Sea area appears to be less involved in these biological phenomena, except for the remarkably high chlorophyll-a concentrations detected next to the Coulman Island coasts during the XIII expedition, while Cape Adare area, considered as the preferred way out of deep and superficial marine currents, remains at low chlorophyll-a levels.

Table 4. Comparison of ELF data collected during the XIII an XVI campaign.

Site	Lat-Lon	Date	Chlorophyll-a [μg/l]	CDOM [Raman un.]
Cape Adare	71°55.93' S - 172°24.01' E	28/12/97	0.36	0.12
		23/01/01	0.40	0.05
Melting area	66°36.16' S - 175° 49.21' E	09/01/98	1.38	0.24
	66°30' S - 179° 50' W	10/01/01	0.50	0.14
Mooring A	76°42.49' S - 169°03.92' E	19/01/00	0.15	0.36
		30/01/01	4.80	0.10
Mooring B	73°59.94' S - 175°46.06' E	18/12/97	0.20	0.21
		19/01/01	0.20	0.16
Mooring D	75°08.46' S - 164°27.26' E	10/12/97	0.96	0.80
		16/01/01	0.20	0.05
Mooring H	75°54.105' S - 177°44.067' W	14/12/97	0.13	0.13
		09/02/01	2.00	0.15
Southern Ocean	54°30.06' S - 174° 59.38' E	12/01/98	0.53	0.03
	54°30' S - 174°00' E	07/01/01	0.40	0.02
Terra Nova Bay	75°51.70'S - 164°11.59'E	03/01/98	2.56	0.43
		08/02/01	2.80	0.13

With the exception of mooring B, the delayed season monitored during the XVI expedition has affected also the characteristics of the offshore seawaters, especially at mooring H, where a diatom bloom was dominating the area. In the same campaign, the highest chlorophyll-a values were monitored in the extremely southern region around mooring A, close to the Ross ice-shelf. As the XIII campaign was characterized by an earlier bloom, in most cases, the increase in the CDOM values (TNB, mooring A and D) support the hypothesis of a post bloom phase, with release of degradation components (i.e. essudates).

The influence of nutrients and biological matter arising from the Antarctic waters has been also observed crossing the polar fronts inside the melting area (66°) and in the Southern Ocean (54°), respectively.

The remote (lidar) and local (spectrofluorometer) chlorophyll-a and CDOM fluorescence data obtained during the XVI Antarctic expedition, including the complete cruise across the Southern Ocean, from the departure (05/01/01) up to the arrival (27/02/01) in New Zealand, have been compared and cross correlated after weekly averaging (Fig. 5). A high correspondence between local and remote data is achieved in all the campaigns. A significantly different trend is observed for the two fluorescent channels: CDOM slowly increases along the crossed seawaters, while chlorophyll-a rise faster after the third week, in correspondence with the algal bloom in the Ross Sea. A final decrease is observed in the return transect as the bloom ended. In general a poor correlation between the two emission channels has been observed. However local correlations seldom occurred for a systematic time shift of five weeks, subsequent to the formation of superficial layers due to the phytoplankton degradation induced by the solar radiation.

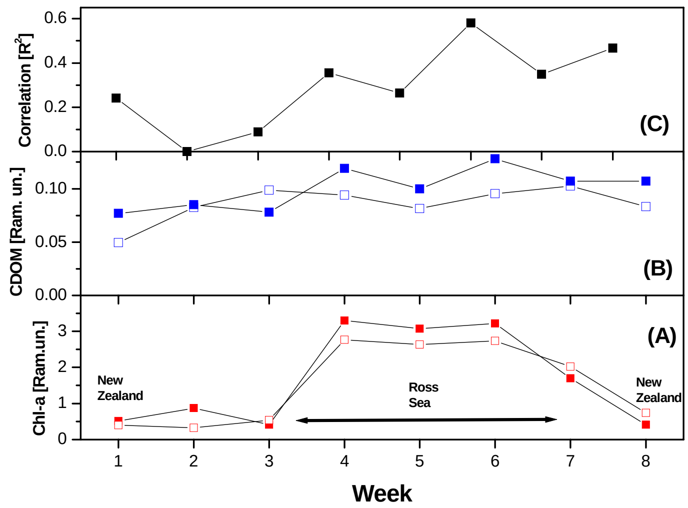

Fig. 5. Comparison between weekly averaged lidar (open square) and spectrofluorometer (filled square) data, collected during the XVI Antarctic expedition (05/01/01-27/02/01). A) chlorophyll-a. B) CDOM. C) chlorophyll-a – CDOM correlation.

3.2 Calibration of SeaWiFS with ELF

Two reasons led us to select the period between 19 and 26 December 1997 for comparing between SeaWiFS to ELF measurements. Firstly, it corresponded to an 8-day L3 [Hooker et al., 1992] SeaWiFS data processing software, and secondly, an algal bloom developed at that time in the Ross Sea, thus exposing the instruments to a broad range of chlorophyll-a concentrations. The 8-day time interval permitted us to make enough simultaneous measurements (216) and the L3 processing level ensured the highest accuracy. Although these choices involved a rather poor granularity (8 days in time, about 9 km × 9 km in space), they have been considered the best compromise for the present analysis. However, the resolution of ELF is substantially different, thus, in order to compare the data, all the ELF measurements falling in a SeaWiFS pixel were averaged, corresponding to a track acquired in about 1 h (length: ~10 km, width: ~20 cm). Notwithstanding the remaining dissimilarity in granularity, the data trend shows a rather satisfactory agreement (Fig. 6): only 4% of them manifestly diverge.

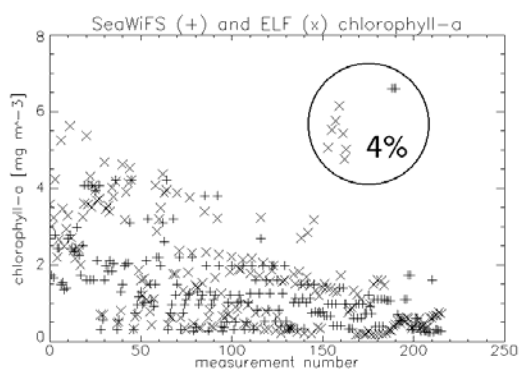

Fig. 6. ELF (+) and SeaWiFS (×) chlorophyll-a concentrations.

The ratio between the chlorophyll-a concentrations measured by ELF and SeaWiFS (Fig. 7), whose mean value is 1.4, suggests that the satellite underestimates chlorophyll-a concentrations relative to the ship, as previously observed by other authors in the same region [Moore et al., 1999]. This is not surprising, because of the taxonomic diversity between phytoplankton in the tropical zones, where the bio-optical algorithm has been calibrated, and Antarctica. In particular, the present observation could be related with the domination of the occurring phytoplankton bloom by *Phaecocystis antarctica* [Arrigo et al., 1998]. Moreover, it could explain why the primary production calculations usually suffer from the “Antarctic paradox” (primary production insufficient to support the population of grazers).

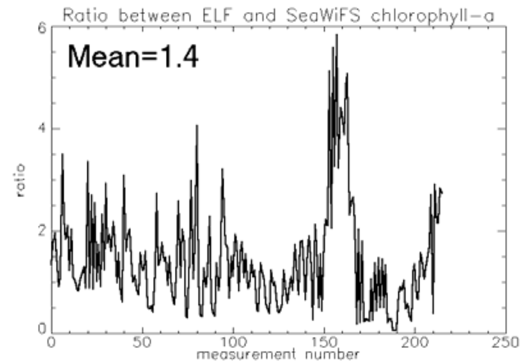

Fig. 7. Ratio between ELF and SeaWiFS chlorophyll-a concentrations.

Fig. 7 and the scatter plot of ELF versus SeaWiFS chlorophyll-a concentrations (Fig. 8) demonstrate that it is not possible to apply a simple correction to the satellite data based on the ship measurements (conversion factor or linear fit). This suggests that the SeaWiFS bio-optical algorithm should be fine tuned in the Southern Ocean with “in situ” data, e.g. with the ELF measurements. In other words, the parameters of the semi-empirical equations used to calculate the chlorophyll-a concentrations from the water-leaving radiances should be calculated from fits on the ship observations.

Bio-optical algorithms can be separated in two main classes: semianalytic and empirical. An evaluation of 2 semianalytic and 15 empirical algorithms, based on a large set of radiance and chlorophyll-a data, demonstrated the best performances of empirical algorithm and supplied the parameters of the equations used to calculate chlor7ophyll-a concentrations from the water-leaving radiances [O’Reilly et al., 1998]. Unfortunately, most of those observations were from nonpolar waters, and thus such parameters should be applied cautiously to the Southern Ocean.

In the following, we focus on the empirical algorithms and we give a preliminary calibration of them for the Ross Sea, based on the ELF measurements. While the SeaWiFS output is the normalized water-leaving radiance (Lwn), the empirical algorithm input is usually the remote sensing reflectance (Rrs). Their relation is given by

$$Lwn(\lambda) = F_0(\lambda) Rrs(\lambda)\,, \tag{3}$$

where λ is the wavelength and F_0 is the mean extraterrestrial solar irradiance. The simplest algorithm (OC1) is expressed by

$$C = 10^{\,a_0 + a_1 R}\,, \tag{4}$$

where C is the chlorophyll-a concentration in mg m^{-3} and, a’s s are constants and

$$R = \log_{10} \frac{Rrs(490\,\mathrm{nm})}{Rrs(555\,\mathrm{nm})}\,. \tag{5}$$

While a modified cubic polynomial function (OC2)

$$C = 10^{\,a_0 + a_1 R + a_2 R^2 + a_3 R^3} + a_4\,, \tag{6}$$

has been chosen as at-launch SeaWiFS operational algorithm, a maximum band ratio method (OC4) gives the best results and is used at present. In this, C is computed using equation (6), but the ratio of formula (5) is taken to be the value which among Rrs(443 nm)/Rrs(555 nm) or Rrs(490 nm)/Rrs(555 nm) or Rrs(510 nm)/Rrs(555 nm) is the greatest. In this way, Rrs(443 nm)/Rrs(555 nm) or Rrs(510 nm)/Rrs(555 nm) replace Rrs(490 nm)/Rrs(555 nm) when the latter is lower and noisier. The former case happens usually for C lower than about 0.3 mg m^{-3}, the latter for C higher than about 1.5 mg m^{-3}.

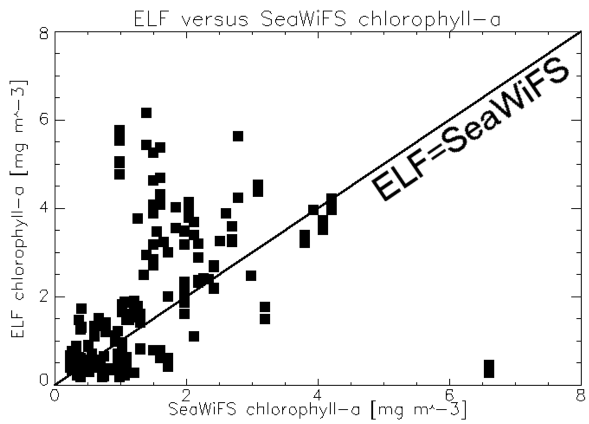

Fig. 8. ELF versus SeaWiFS chlorophyll-a concentrations.

The scatter plot of ELF chlorophyll-a concentrations versus SeaWiFS band ratios (Fig. 9) shows a large dispersion of the experimental points. As a consequence, the linear fit (OC1) has been chosen. It does not seem reasonable to use higher order functions, as confirmed by the unstable behavior of the corresponding fits. The ELF-calibrated OC1, standard OC1 and OC2 bio-optical algorithm, as well as SeaWiFS chlorophyll-a concentrations (representing the OC4 bio-optical algorithm) versus SeaWiFS band ratios are also displayed in Fig. 9. The parameters of the above mentioned algorithms are summarized in Table 5. Let us note that the difference between ELF-calibrated and standard OC1 is statistically significant.

Table 5. Parameters of some bio-optical algorithms for SeaWiFS.

	a_0	a_1	a_2	a_3	a_4
Standard OC1	0.3734	-2.4529			
OC2	0.3410	-3.0010	2.8110	-2.0410	-0.0400
OC4	0.4708	-3.8469	4.5338	-2.4434	-0.0414
ELF-calibrated OC1	0.325 ± 0.026	-2.27 ± 0.14			

Fig. 9 suggests that standard OC1 and OC2 overestimate the higher concentrations (more than about 0.5 mg m^{-3} for standard OC1 and 2 mg m^{-3} for OC2) and underestimates the lower concentrations, especially around 1 mg m^{-3} for OC2. The switching among Rrs(490 nm)/Rrs(555 nm), Rrs(443 nm)/Rrs(555 nm) and Rrs(510 nm)/Rrs(555 nm) explains the dispersion of SeaWiFS chlorophyll-a concentrations versus SeaWiFS band ratios. In general, the SeaWiFS measurements (×) are lower than the ELF-calibrated bio-optical algorithm (continuous line), as we expected from the comparison between SeaWiFS and ELF data.

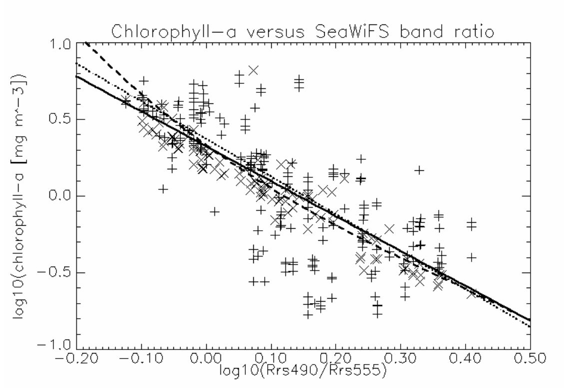

Fig. 9. ELF (+) and SeaWiFS (×) chlorophyll-a concentrations versus SeaWiFS band ratios. The continuous, dotted and dashed lines represent ELF-calibrated OC1, standard OC1 and OC2 bio-optical algorithms, respectively. The SeaWiFS chlorophyll-a concentrations versus SeaWiFS band ratios represent the OC4 bio-optical algorithm.

Finally, the ELF-calibrated bio-optical algorithm was applied to the water-leaving radiances measured by SeaWiFS in order to obtain corrected chlorophyll-a concentrations (Fig. 11) that can be compared to the original values (Fig. 10). Their difference (Fig. 12) is around zero in open ocean waters and of about 20% in the Ross Sea. This is an attractive performance of the ELF-calibrated bio-optical algorithm, allowing its application in the whole Southern Ocean.

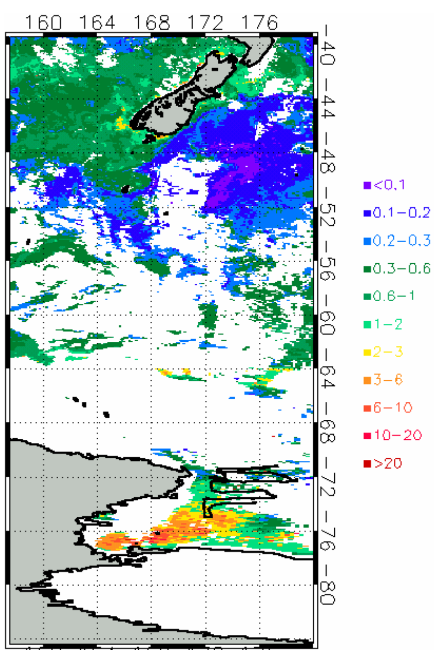

Fig. 10. SeaWiFS chlorophyll-a concentrations (OC4 algorithm). Black line: ship track.

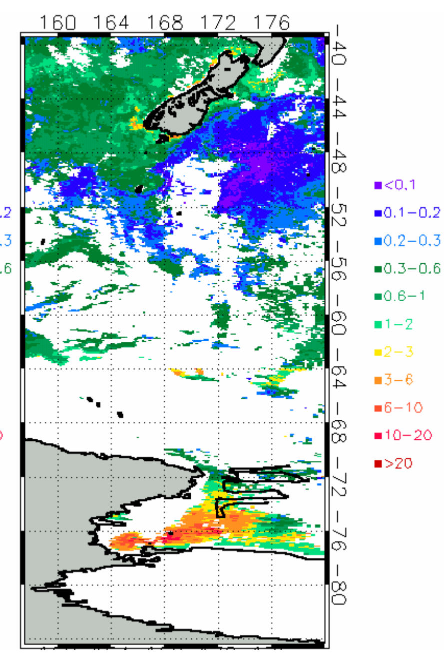

Fig. 11. SeaWiFS chlorophyll-a concentrations (ELF-calibrated OC1 algorithm). Black line: ship track.

4. Conclusions

The active and passive remote sensing of the ocean has been reviewed describing a satellite radiometer (SeaWiFS) and introducing a lidar fluorosensor (ELF). The measurements of chlorophyll-a and CDOM collected by ELF during two oceanographic campaigns have been presented. From their discussion, the main features of phytoplankton blooms (geographic extension, pre- and post-bloom stages, dominant composition of the algal assemblage, etc.) and of their seasonal dynamics could be outlined. Moreover, the correlation analysis of the fluorescence spectra clarifies the relationship between phytoplankton and CDOM in Antarctic waters.

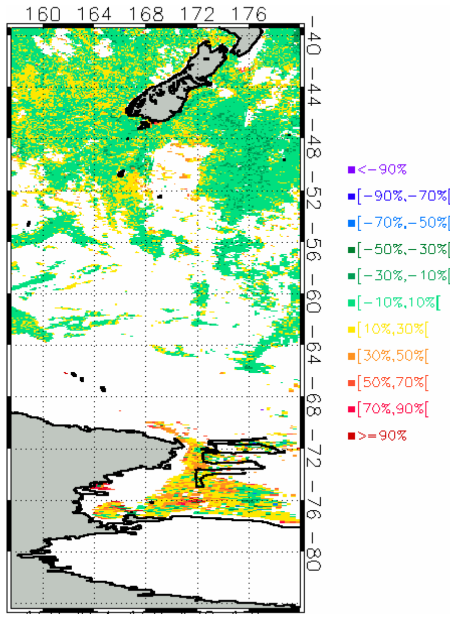

Fig. 12. Difference between SeaWiFS chlorophyll-a concentrations calculated with OC4 and ELF-calibrated OC1 algorithms. Black line: ship track.

Comparing SeaWiFS and ELF data in the Ross Sea has shown that the satellite underestimates chlorophyll-a concentrations relative to the ship. This discrepancy is not surprising due to the taxonomic diversity between phytoplankton characterizing calibration and measurement zones. In order to improve the agreement, the SeaWiFS bio-optical algorithm has been fine tuned in the Ross Sea with the ELF data. Results could be satisfactory in the whole Southern Ocean. The coverage of SeaWiFS and the accuracy of ELF have been merged to obtain a better understanding of the Antarctic marine environment and, especially, of its biomass processes.

Acknowledgements

This work has been supported by the Italian Antarctic Research Program (PNRA), Technology Sector, 5b1 Lidar Fluorosensor and 11-5 Palucc5 Projects (for the periods 1996-1998 and 1999-2001, respectively). The authors would like to thank the SeaWiFS Project (Code 970.2) and the Distributed Active Archive Center (Code 902) at the Goddard Space Flight Center, Greenbelt, MD 20771, for the production and distribution of these data, respectively. These activities are sponsored by NASA's Mission to Planet Earth Program.

We are grateful to F. Parmiggiani for helpful discussions and to P. D'Angelo and F. Simoni for computing assistance. The contribution of M. Galli to the data processing is kindly acknowledged.

References

[1] K. R. Arrigo, D. H. Robinson, D. L. Worthen, B. Schieber, M. P. Lizotte, Bio-optical properties of the southwestern Ross Sea. J. Geophys. Res. C, **103**, 21683-21695 (1998).

[2] R. Barbini, F. Colao, R. Fantoni, A. Palucci, S. Ribezzo, C. Micheli Design and application of a lidar fluorosensor system for remote monitoring of phytoplankton. ICES J. Mar. Sci., **55**, 793-802 (1998).

[3] R. Barbini, F. Colao, R. Fantoni, A. Palucci, S. Ribezzo, Shipborne laser remote sensing of the Venice lagoon. Int. J. Rem. Sens., **20**, 2405-2421 (1999).

[4] R. Barbini, F. Colao, R. Fantoni, A. Palucci, S. Ribezzo, Differential lidar fluorosensor system

used for phytoplankton Bloom and seawater quality monitoring in Antarctica. Int. J. Rem. Sens., **22**, 369-384 (2001)

[5] M. Bristow, D. Nielsen, D. Bundy, R. Furtek, Use of Raman emission to correct airborne laser fluorosensor data for effects of water optical attenuation, Appl. Opt., **20**, 2889-2906 (1981).

[6] C. A. Carlson, D. A. Hansell, E. T. Pelzer, W. O. Smith, Stock and dynamics of dissolved and particulate organic matter in the Ross Sea, Antarctica, Deep-Sea Res. II, **47**, 3201-3225 (2000).

[7] D. J. Carlson, L. M. Mayer, Enrichment of dissolved phenolic organic material in the surface mi crolayer of coastal waters, Nature, **286**, 482-483 (1980).

[8] A. M. Chekalyuk, M. Yu. Gorbunov, Lidar in situ study of sun light regulation of phytoplankton photosynthetic activity and chlorophyll fluorescence. Proc. SPIE **1922**, 421-427, (1993).

[9] A. P. Cracknell, S. K. Newcombe, A. F. Black, N. E. Kirby, The ABDMAP (Algal Bloom De tection, Monitoring and Prediction) Concerted Action. Int. J. Rem. Sens., **22**, 205-247, (2001).

[10] H. Edner, J. Johansson, P. Ragnarson, S. Svanberg, E. Wallinder, Remote monitoring of vegeta tion using a fluorescence lidar system in spectrally resolved and multi-spectral imaging modes. EARSeL Adv. Rem. Sens., **3**, 198-206 (1995).

[11] C. Elachi, Introduction to the Physics and Techniques of Remote Sensing, Wiley, New York (USA), (1987).

[12] P. G. Falkowski, J. A. Raven, Aquatic photosynthesis. Blackwell, Malden (USA), (1997).

[13] L. Fiorani, S. Mattei, S. Vetrella, Laser methods for the atmospheric correction of marine radi ance data sensed from satellite. Proc. SPIE **3496**, 176-187, (1998).

[14] H. R. Gordon, M. Wang, Retrieval of water-leaving radiance and aerosol optical thickness over the oceans with SeaWiFS: a preliminary algorithm. Appl. Opt., **33**, 443-452, (1994).

[15] F. E. Hoge, R. N. Swift, Airborne simultaneous spectroscopic detection of laser induced water Raman backscatter and fluorescence from chlorophyll a and other naturally occurring pigments. Appl. Opt., **20**, 3197-3205 (1981).

[16] S. B. Hooker, W. E. Esaias, G. C. Feldman, W. W. Gregg, C. R. McClain An overview of SeaWiFS and ocean color. In “SeaWiFS Technical Report Series – Technical Memorandum 104566.” S.B. Hooker and E.R. Firestone, eds., NASA, Washington, (USA) vol. **1**, (1992).

[17] C. Koechler, J. Verdebout, G. Bertolini, A. Gallotti, G. Zanzottera, L. Fiorina, Determination of aquatic parameters by time resolved laser fluorosensor operating from helicopter. Proc. SPIE, **1714**, 93-107, (1992).

[18] M. Innamorati, G. Mori, L. Massi, L. Lazzara, C. Nuccio, Phytoplankton biomass related to envi ronmental factors in the Ross Sea. In “Ross Sea Ecology. Italian Antarctic Expeditions (1987-1995).” F. Faranda, L. Guglielmo and A. Ianora, eds., Springer, Berlin (Germany) pp. 217-230, (1999).

[19] L. Lazzara, V. Saggiomo, M. Innamorati, O. Mangoni, L. Massi, G. Mori, C. Nuccio, Photosynthetic parameters, irradiance and production estimates in the western Ross Sea. In “Ross Sea Ecology. Italian Antarctic Expeditions (1987-1995).” F. Faranda, L. Guglielmo and A. Ianora, eds., Springer, Berlin (Germany) pp. 259-273 (1999).

[20] R. M. Measures, Laser Remote Sensing, Krieger, Malabar (USA), (1992).

[21] J. K. Moore, M. R. Abbott, J. G. Richman, W. O. Smith, T. J. Cowles, K. H. Coale, W. D. Gardner, Barber R.T., SeaWiFS satellite ocean color data from the Southern Ocean. Geophys. Res. Lett., **26**, 1465-1468 (1999).

[22] M. Olaizola, R. J. Geider, W. G. Harrison, L. M. Graziano, G. M. Ferrari, P. M. Schlittenhardt Synoptic study of variations in the fluorescence-based maximum efficiency of photosynthesis across the North Atlantic Ocean. Limnol. Oceanogr., **41**, 755-765 (1996).

[23] J. E. O’Reilly, S. Maritorena, B. G. Mitchell, D. A. Siegel, K. L. Carder, S. A. Garver, M. Kahru, C. McClain, Ocean color chlorophyll algorithms for SeaWiFS. J. Geophys. Res. C, **103**, 24937-24953. (1998)

[24] R. Reuter, D. Diebel, T. Hengstermann, Oceanographic laser remote sensing: measurements of hydrographic fronts in the German Bight and in the northern Adriatic Sea. Int. J. Rem. Sens., **14**, 823-848 (1993).

[25] S. Sathyendranath, G. Cota, V. Stuart, H. Maass, T. Platt, Remote sensing of phytoplankton pig ments: a comparison of empirical and theoretical approaches. Int. J. Rem. Sens., **22**, 249-273 (2001).

[26] W. O. Smith, D. M. Nelson, G. DiTullio, A. R. Leventer, Temporal and spatial patterns in the Ross Sea: phytoplankton biomass, elemental composition, productivity and growth rates. J. Geo phys. Res. C, **101**, 18455-18466 (1996).